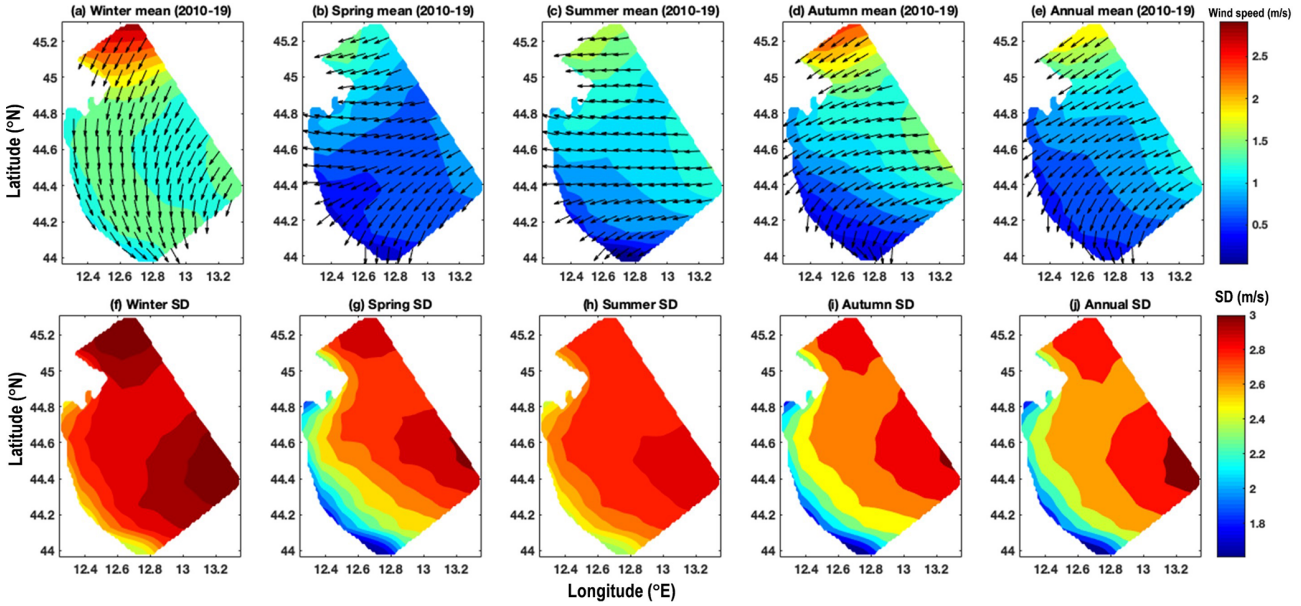

Figure 4. Wind climatology for the Emilia-Romagna region based on ECMWF analysis wind data for 2010 to 2019. Mean wind speed and direction for **(a)** winter, **(b)** spring, **(c)** summer, **(d)** autumn, and **(e)** annual periods (top panels). The lower panels show the standard deviation (SD) of wind speed for **(f)** winter, **(g)** spring, **(h)** summer, **(i)** autumn, and **(j)** annual periods.

To better study the wind characteristics along the ER coast, the wind rose diagrams are shown for the eight control points in Fig. 5a to h. Points 1 to 5, belonging to Zone A and Zone B, have the highest wind speeds, approaching at an angle of 45 to 135°. The wind speed ranging from 3 to 4 m s^{-1} is more frequent at these control points at an approaching angle ranging from 45 to 90°. The average coastal angles of Zone A and Zone B are nearly 45°. Points 6 to 8 fall along the concave side of the coastal area, i.e. in Zone C. Along these control points, the maximum wind speed approaches from W to NNW. The wind speeds up to 3.5 m s^{-1} show a marked increase in frequency. The frequent wind speeds approach from NW and ENE for station 6, NNE for point 7, and NNW for point 8. Moving from point 1 to 8, there is a gentle shift in the maximum wind speed approaching from NNE to ENE.

4.2 Wave climatology of the Emilia-Romagna coast

4.2.1 Wave height and direction climatology

Figure 6 (top panels) depicts the annual mean H_s for the ER coast and the seasonal H_s means for winter, spring, summer, and autumn. The SD for each event is illustrated in the bottom panels from 2010 to 2019. The waves converge at the southern and the northern part of the study domain due to the shape of the coastline. There is divergence in wave energy in the middle region of the coastal domain (i.e. Zone B as reported in Fig. 1c). The annual H_s mean (Fig. 6e) in the domain varied from 0.08–0.6 m. The annual average H_s is higher (0.5–0.7 m) off the ER coast and at the boundary in the open ocean, and in the central ER domain H_s is of the order of 0.5–0.6 m. However, in the ER coastal belt, the annual mean H_s is < 0.4 m owing to the bathymetric features.

The seasonal climatology of H_s in the winter season (Fig. 6a) indicates higher waves offshore of the order of 0.1–0.9 m, where the ER coastal belt has $H_s < 0.5$ m. In spring (Fig. 6b) and summer (Fig. 6c) the H_s values are comparatively lower and vary in the range of 0.1–0.5 and 0.1–0.33 m respectively. The autumn H_s mean in the ER coastal belt is < 0.4 m. The spatial H_s field structure and direction approximately resemble the bathymetric contour lines (Fig. 1b). The annual SD (Fig. 6j) varies from 0.09–0.71 m in the ER domain. The summer season (Fig. 6h) shows the lowest SD (0.1–0.38 m) compared to all other seasons.

The detailed features of the model in the coastal zone are shown by means of wave rose diagrams (Fig. 7) for the eight points in Fig. 1c. The waves at control point 1 fall in the Lido di Pomposa region where the coast is sheltered and exposed to winds and marine currents. The bathymetric contour enables the waves to converge in control point 1, where the maximum wave heights approach from E to SE. From points 2 to 7 along Porto Garibaldi to Rimini, the approaching angles of wave heights are from NE to SE. The maximum waves approach from ENE to E for points 2 to 4 and NE to E for points 5 to 8. The maximum wave activity is observed at point 3. Point 1 is a relatively calm area compared to the other control points, perhaps because of the shadow zone. The concave shape of the coast, well represented by the high-resolution unstructured-grid model, and bathymetric patterns

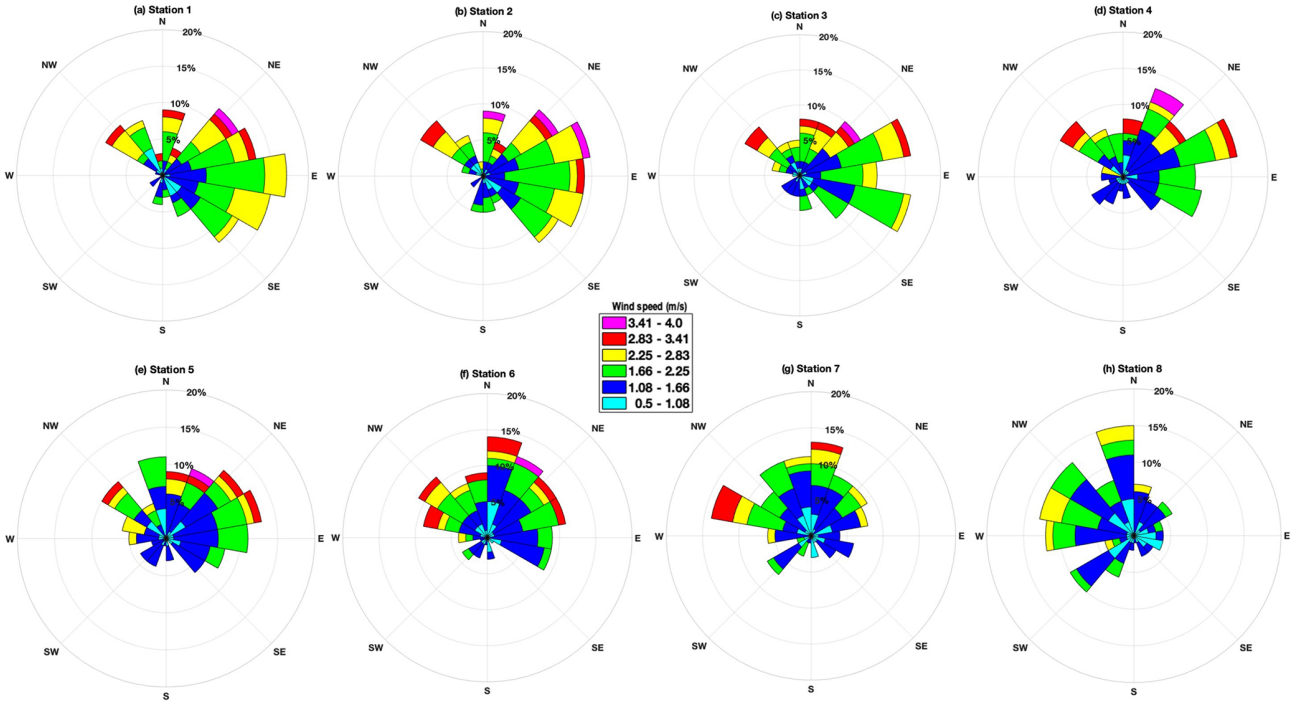

Figure 5. Wind rose diagrams at the control points shown in Fig. 1 based on monthly average winds throughout 2010–2019. The wind rose shows the direction the winds come from (N: north; NE: northeast; E: east; SE: southeast; S: south; SW: southwest; W: west; NW: northwest).

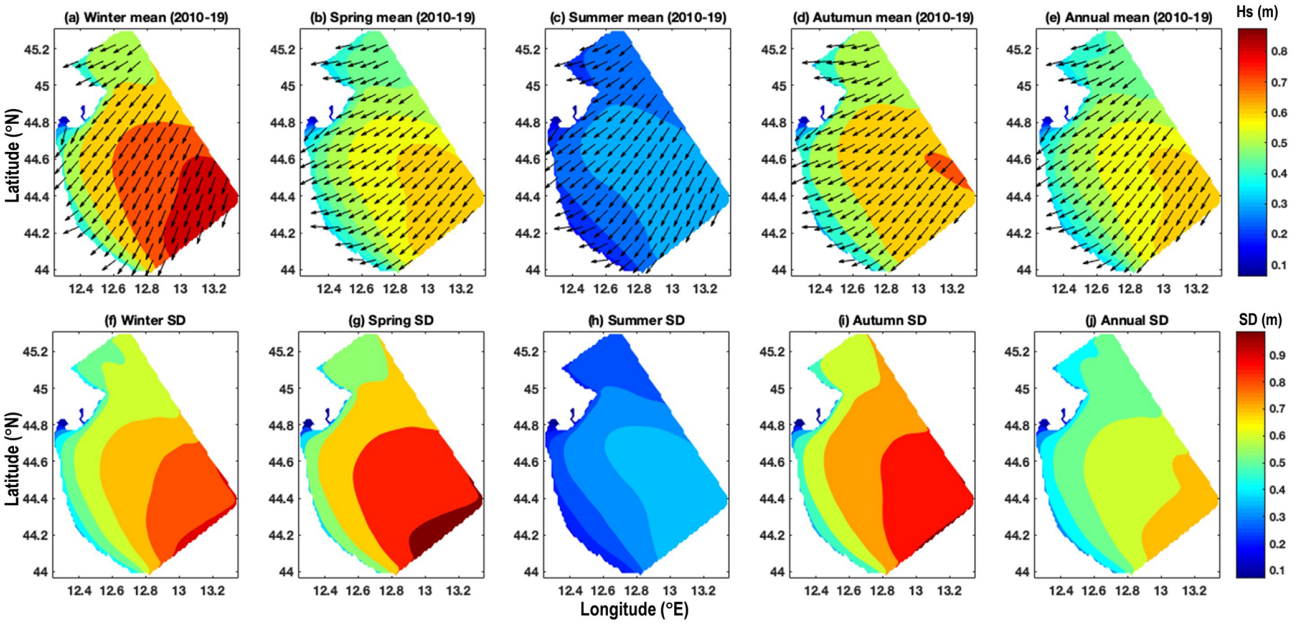

Figure 6. Wave climatology for the Emilia-Romagna region for 2010 to 2019. Mean significant wave height and direction for **(a)** winter, **(b)** spring, **(c)** summer, **(d)** autumn, and **(e)** annual (top panels). The lower panels show the standard deviation (SD) of wave height for **(f)** winter, **(g)** spring, **(h)** summer, **(i)** autumn, and **(j)** annual periods.

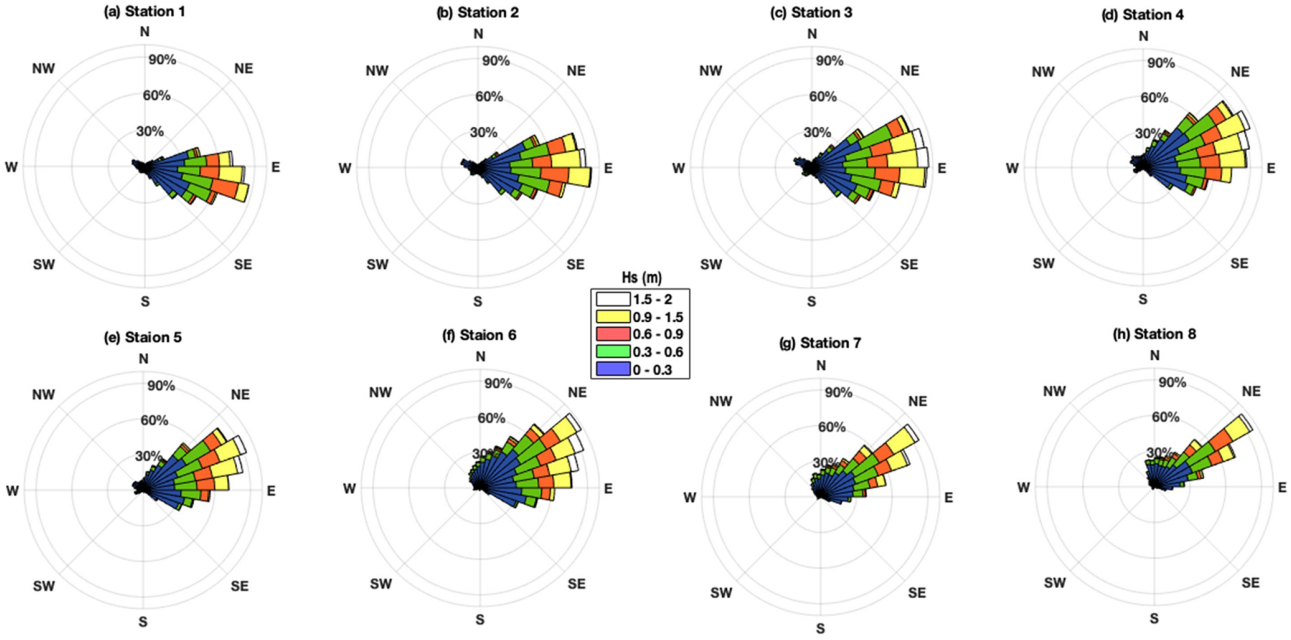

Figure 7. Nearshore wave climate: wave rose diagrams in the coastal belt of Emilia-Romagna along control points 1 to 8 (see Fig. 1c). The wave rose indicates the direction the waves come from (N: north; NE: northeast; E: east; SE: southeast; S: south; SW: southwest; W: west; NW: northwest).

are key to understanding the prevailing wave characteristics in the ER coastal belt. The wave energy converges at the end points and diverges at the middle points.

Based on available buoy data for the Cesenatico station, the observed wave roses are compared with the model estimates for selected years as shown in Fig. 8. Overall, the modelled wave roses (Fig. 8b, d, and f) show reasonable correspondence with the observed data (Fig. 8a, c, and e), even with some difference in magnitudes. An underestimation of model wave heights in the lower ranges is noted. Comparing the directional distribution of waves, the directions are comparable and in the same sectors but there exist higher differences in their magnitudes. A similar wave climate by the Nausicaa buoy located offshore of Cesenatico is reported in studies by Armaroli et al. (2012) and Romagnoli et al. (2021), which shows that this is the representative wave climate of the Emilia-Romagna coast. This qualitative comparison shows that at the Cesenatico station, overall characteristics of waves are fairly reproduced by the model.

Figure 9 shows the offshore wave climate, presented as wave rose diagrams at the control points along the boundaries of the study domains (control points 9 to 14). In Fig. 9a at point 9, the waves approach from NE to SE with maximum H_s approaching from ENE to ESE. At point 10, the predominant waves are at an angle of 30 to 150° where the maximum H_s approaches from NE and SE directions (see Fig. 9b). For points 11 to 14, the predominant wave directions are from 30 to 150°, where the maximum H_s approaches from NE and SE directions. Deep-water control points 10 to 14 receive waves from all directions.

4.2.2 Wave spectra characteristics

In the ER region, there are hardly any studies on the spectral characteristics of the waves. Cavaleri et al. (2019) analysed model spectra for the event of 29 October 2018 in the northern Adriatic Sea and compared them with measurements on the Venice coastline. The simulated wave spectra on the 25th of the months corresponding to winter (February), spring (May), summer (August), and autumn (November) at 12:00 LT are represented in Fig. 10a to d for station 6 for 2010–2019.

Figure 10a shows the simulated instantaneous spectra in February (25th of the month, 12:00 LT) with the highest peak energy of 2.0234 $m^2\,Hz^{-1}$ for 2018 and the lowest of 0.0008 $m^2\,Hz^{-1}$ for 2012 and 2014. February, which is a representative month of the winter season, shows a combination of single-peaked and double-peaked spectra with swell dominance at the coastal location. In all the seasons, the swell dominates the spectral energy with a peak at around 0.11 Hz (9 s). The shorter wave peaks range from 0.21 to 0.54 Hz (1.8 to 4.7 s). The spectra vary considerably over the years, and in general, the wave spectra at the Cesenatico coastal location showed signatures of single- and double-peaked spectra for the period 2010–2019 (Table 5). The wave spectra were prominently double-peaked during all seasons (45 %–53 %), along with single-peaked spectra but with a lower percent-

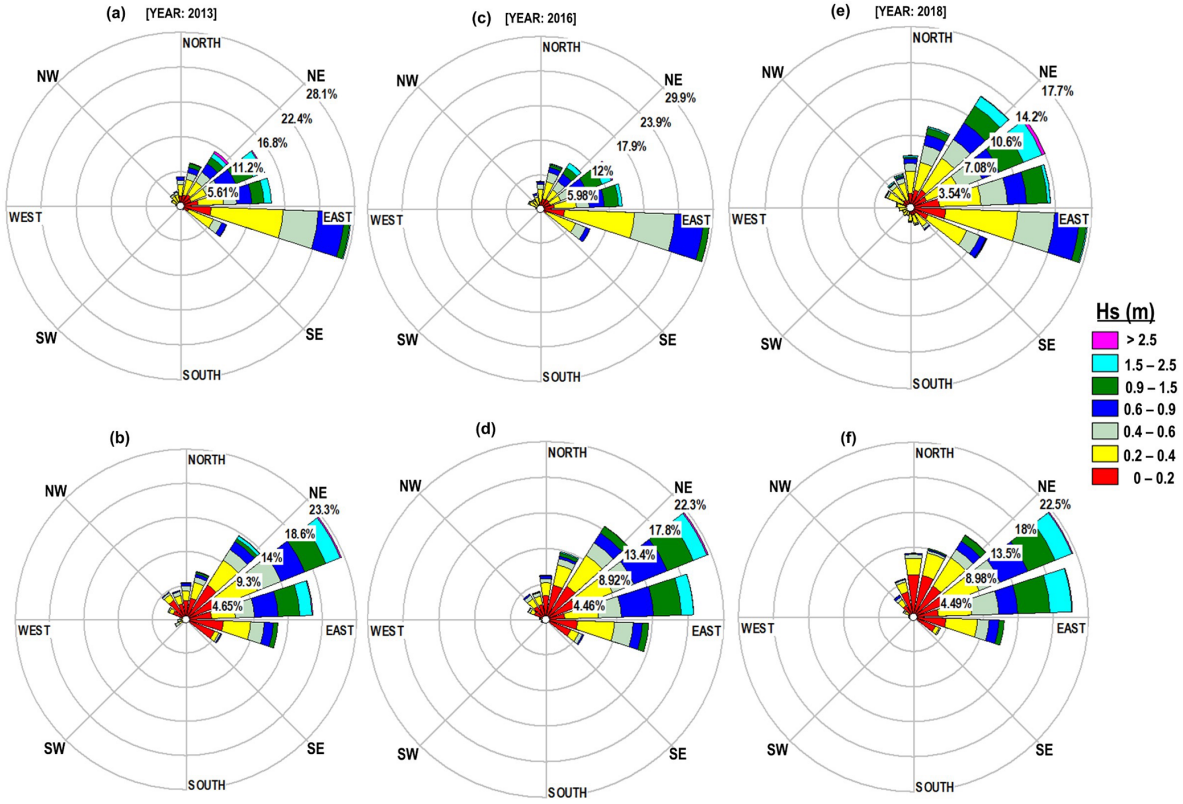

Figure 8. Comparison of directional histograms of wave heights: buoy **(a, c, e)**, and simulated **(b, d, f)** data at Cesenatico, station 6 (NE: northeast; SE: southeast; SW: southwest; NW: northwest).

Table 5. Number of occurrences of single-peaked, double-peaked, and multi-peaked spectra at Cesenatico location for different seasons (2010–2019).

Seasons (2010–2019)	Single peak (%)	Double peak (%)	Multi-peak (%)
Winter	31	45	24
Spring	32	45	23
Summer	27	53	20
Autumn	33	49	18

age of occurrences (27 %–33 %). Double peakedness was highly prominent in the summer season (53 %), while winter, spring, and autumn showed dominance of single-peaked spectra (31 %–33 %). As evident from Table 5, the percentages of the number of peaks (single/double) in the Cesenatico location clearly depict the co-existence of sea-swell characteristics in the study domain.

The monthly mean wave spectra for winter, spring, summer, and autumn corresponding to the typical months of February, May, August, and November for 2010–2019 are represented in Fig. 11a to d. During February (Fig. 11a), the averaged spectra showed prominent single peaks for most of the years with peak energies of the order of 0.1615–0.722 $m^2\,Hz^{-1}$. The highest peak energies were in 2012 (0.701 $m^2\,Hz^{-1}$) and 2014 (0.722 $m^2\,Hz^{-1}$), and during the 10-year period the peak frequencies ranged from 0.0974 to 0.1726 Hz. Figure 11b shows the averaged spectral characteristics for May (spring). As seen from Fig. 11b, 2019 had the highest peak energies of 0.253 $m^2\,Hz^{-1}$, and the spectra also highlight a few secondary peaks in some of the years with the peak frequency ranging from 0.1072 to 0.2297 Hz. During the summer season (August), the spectra show single/double peaks with peak energies varying from 0.0102 to 0.0686 $m^2\,Hz^{-1}$ (Fig. 11c). The maximum peak energy was for 2016 (0.0686 $m^2\,Hz^{-1}$) with comparatively low energies for the rest of the years and with peak frequencies varying from 0.1427 to 0.278 Hz. Similarly, during autumn (Fig. 11d), the averaged spectra were mostly single-peaked with peak energies of the order of 0.1362 to 0.740 $m^2\,Hz^{-1}$. The highest peaks with energies of 0.740 $m^2\,Hz^{-1}$ were in 2019, with the lowest energy in 2015. The dominant frequencies corresponding to the peak energies were 0.0974–0.2089 Hz.

Overall, the highest and lowest spectral peaks are in winter and summer, with energies of 0.722 and 0.0686 $m^2\,Hz^{-1}$, as shown in Fig. 11a and c. The mean wave spectra for 2010

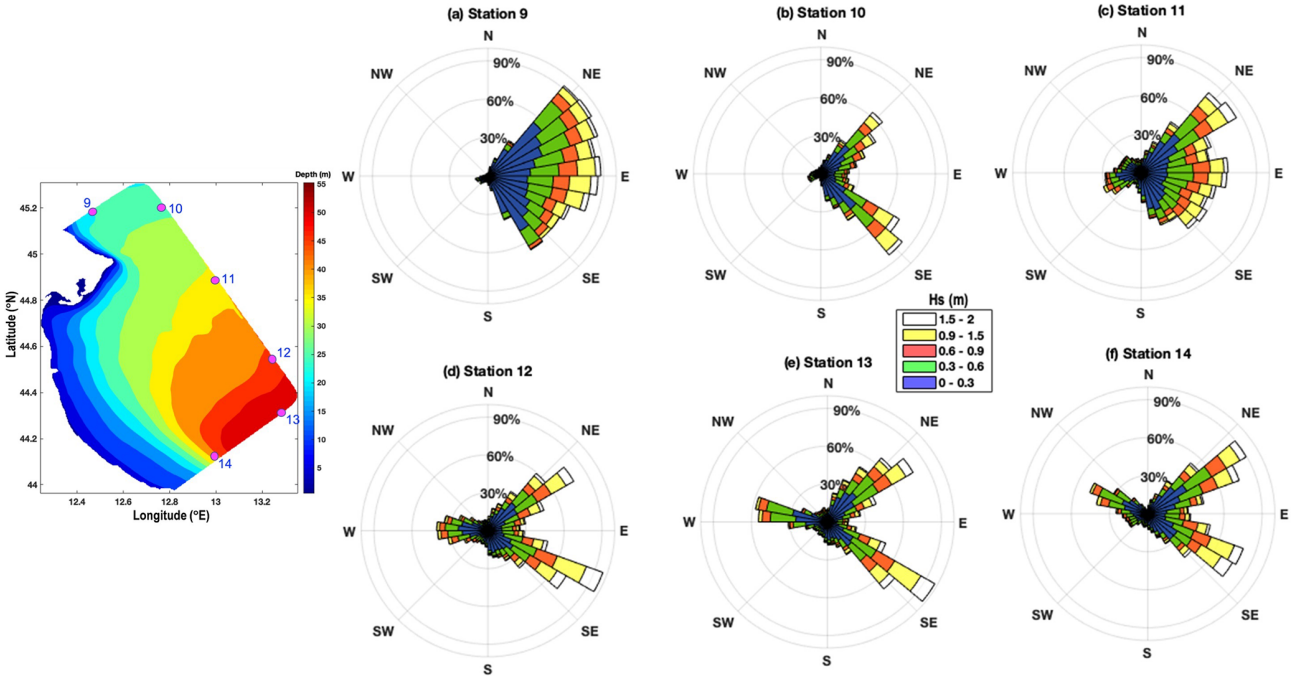

Figure 9. Offshore wave climate: wave rose diagrams in the boundaries of the model domain for the control points (9 to 14) as indicated in the location bathymetric map shown adjacently (left) (N: north; NE: northeast; E: east; SE: southeast; S: south; SW: southwest; W: west; NW: northwest).

to 2019 exhibit a peak in variance for 2014, 2019, 2016, and 2019 for winter, spring, summer, and autumn respectively. The spectra show more or less similar characteristics for spring and autumn. There is also a reversal of spectrum curves for winter and spring as swells clearly dominate the coastal location. The spreading of spectra, which is dependent upon the wind characteristics and the prevailing fetch, is variable during all seasons.

4.2.3 Wavelet analysis

Wavelet analysis is an important tool to analyse spectral components and occurrence time (Torrence and Compo, 1998). The wavelet considers spectral components' time localization, as well as time–frequency rendering of signal into realization, such that the frequencies in the wavelet analysis are associated with the time domain. Thus, wavelet analysis (based on the Morlet mother wavelet) provides an understanding of spectral characteristics and their variability in time.

In this study the wavelet transform for H_s (Fig. 12) was applied to the coastal location of Cesenatico for 2010–2019, using the mean model estimates. Figure 12a represents the wavelet power, with the x axis representing the time and y axis denoting the component periods. Figure 12b represents the global wavelet power spectrum, i.e. time-averaged power spectrum, which uses the same y axis. Cesenatico was selected as it was the station where the wave parameters were validated with the model estimates. The idea of presenting the wavelet transform is to accurately represent the variance in the spectrum. In the power wavelet (Fig. 12a), the real signals can be observed enclosed in the black contours with a 95 % confidence level, while the region below the dashed magenta line indicates the cone of influence, in which the time series analysis edge effects are significant. In the global spectrum, the peaks indicate the combined signal throughout the analysis. The dashed red line in the global spectrum corresponds to a confidence level of 95 %.

In Fig. 12, the largest signal occurs in the 256–512 d band, which contains the seasonal frequency, and sporadic signals can be identified by comparatively short times (2–3 months). Figure 12a indicates that over the 10-year period, intermittent oscillations are in band 16–128 in the years 2011, 2012, 2014, 2016, 2018, and 2019. Figure 12c shows the 16–512 d period of the scale average H_s time series, with 95 % significance denoted by a dashed red line. Significant peaks can be seen in 2014, 2015, 2016, and 2019, while 2019 shows the highest variance. From 2010 to 2013 and 2017 to 2018, the peaks showed lower amplitudes. The seasonal signal is very different from year to year with peaks occurring sometimes only during the autumn.